Cheng, Y. P., Nakata, Y. & Bolton, M. D. (2003). *Géotechnique* **53**, No. 7, 633–641

Discrete element simulation of crushable soil

Y. P. CHENG*, Y. NAKATA† and M. D. BOLTON*

Computer simulations of crushable agglomerates were performed using the PFC^{3D} computer code, which adopts the distinct element method (DEM). Agglomerates were made by bonding elementary spheres in 'crystallographic' arrays, and by giving each sphere an existence probability of 0·8. Weibull statistics of the crushing strength of the resulting agglomerates, when tested singly between parallel platens, matches that of real silica sand grains. Triaxial tests on a cubical sample made of 389 agglomerates were then simulated. Curves of isotropic compression are shown, and the effect of loading rate on the position of the compression curves is discussed in relation to the practical question of performing DEM simulations as fast as possible without creating inertia errors. Other stress paths, including conventional 'drained' triaxial compression, constant mean effective stress, and constant-volume paths, were also simulated from different initial stresses along the virgin e–$\log p'$ curve. The numerical results are compared quantitatively with the testing data of the silica sand. They are also discussed in relation to characterising crushable soils during normal compression, yield, and critical states. Simulation of crushable soils using DEM provides valuable insights concerning the micromechanical origins of soil plasticity.

KEYWORDS: compressibility; numerical modelling; particle crushing/crushability; sands; shear strength; statistical analysis

Des simulations par ordinateur d'agglomérats sujets au broyage ont été effectuées en utilisant le logiciel PFC^{3D} qui adopte la méthode des éléments distincts (DEM). Les agglomérats ont été fabriqués en rassemblant des sphères élémentaires en structures 'cristallographiques' et en donnant à chaque sphère une probabilité d'existence de 0.8. Les statistiques de Weibull sur la résistance au broyage des agglomérats résultants, qui sont testés un par un entre des plaques parallèles, correspondent à celles des grains de sables siliceux réels. Nous avons alors simulé des essais triaxiaux sur un échantillon cubique constitué de 389 agglomérats. Nous présentons les courbes de compression isotrope et nous étudions l'effet de la vitesse de chargement sur la position des courbes de compression sous un angle pratique : arriver à mener des simulations DEM aussi rapidement que possible sans créer d'erreurs d'inertie. D'autres chemins de contrainte, incluant celui de compression triaxiale 'drainée', celui à contrainte moyenne effective constante et celui à volume constant ont également été simulés à partir de différentes contraintes initiales le long de la courbe vierge e–$\log p'$. Nous comparons les résultats numériques de manière quantitative avec les données des essais sur le sable siliceux. Ces résultats sont également étudiés afin de caractériser les sols sujets au broyage lors d'une compression normale, à la rupture et à l'état critique. Les simulations de sols sujets à l'écrasement, utilisant la méthode DEM, donnent des informations précieuses sur les origines micromécaniques de la plasticité des sols.

INTRODUCTION

The crushability of sand has been investigated experimentally by a number of researchers. Triaxial testing of sands shows a strong dependence of strength and dilatancy behaviour on both relative density and stress level, relating to grain crushability (Bolton, 1986). An empirical characterisation of the peak angle of internal friction of sands in relation to these two parameters was reasonably successful, although inherent anisotropy due to bedding was also seen to be important (Hoque *et al.*, 1996). The tendency to either contract or dilate during undrained shearing is also essential in studying pore pressure generation and possible liquefaction in monotonic tests on very loose sands (Castro & Poulos, 1977), or in cyclic tests on any loose to medium-dense sand (Ishihara *et al.*, 1975), but the importance of stress level has often not been given sufficient attention.

In view of the importance of soil crushability to stress-level effects, further studies have been carried out to understand the statistics of individual grain breakages. Results of single-particle crushing tests have been compared with the one-dimensional compression of samples of the same uniformly graded sand (Nakata *et al.*, 2001). They showed crushing and irrecoverable compression in a sand sample at a macroscopic stress level much smaller than that required to break individual grains, and attributed this to the unequal distribution of internal contact forces within an aggregate of grains. Cheng *et al.* (2001) observed particle breakage through a glass platen when sands were compressed inside a mini-oedometer. The initial breakage under very small macroscopic stresses must have depended on the existence of strong 'chains' of contact forces acting on some individual grains in particular packing structures. They confirmed that two phases of breakage could be described: an initial phase governing the onset of breakage of individual grains, and a second phase in which broken fragments continued to break as 'normal compression' was exhibited.

The comprehension of stress and density effects in a general framework for the behaviour of sands has been under way for many years. Been & Jefferies (1985) defined a state parameter in relation to the difference between the current voids ratio and the critical voids ratio at the same mean effective stress. Yasufuku & Hyde (1995) and Cuccovillo & Coop (1999) went further in aiming to establish a critical-state framework for sand behaviour, which began to clarify the relationship between yield and crushability. This paper aims to contribute to the general discussion of soil plasticity by attempting to simulate crushable soil behaviour using discrete element simulation.

Discrete element simulation (DEM) of perfectly elastic and infinitely strong grains provides many insights into the deformation of granular media (Thornton, 2000). Qualitative

Manuscript received 10 October 2002; accepted 24 March 2003. Discussion on this paper closes 1 March 2004, for further details see p. ii.

* Department of Engineering, Cambridge University, UK.
† Department of Civil Engineering, Yamaguchi University, Japan; Visitor, Department of Engineering, Cambridge University, UK.

agreement of the mechanical behaviour between the simulated results and real sand was found, yet the stress level dependence of granular behaviour could not properly be represented because the crushability of sand was ignored. New theoretical frameworks link 'plastic yielding' and 'plastic hardening' of sands with the successive breakage of grains (McDowell *et al.*, 1996; McDowell & Bolton, 1998), and draw attention to the need for a 'clastic mechanics' of brittle grains subject to both rearrangement and breakage. Robertson (2000) went on to simulate crushable grains in DEM by making agglomerates of bonded microspheres. Robertson & Bolton (2001) provided a realistic investigation of both stress level and stress path dependence in crushable sand. They showed in one-dimensional compression that $K_{0,nc}$ changed from about 0·2 for unbreakable grains with hard elastic contacts to about 0·5 as grains crushed, implying that the empirical use of $K_{0,nc} = 1 - \sin\phi$ depends on particle crushing. They also identified contours of breakage that resembled conventional yield surfaces on a (q, p') stress-path diagram.

In this paper, similar simulations are quantitatively compared with real data for silica sand. Good comparisons with single-particle crushing data and isotropic compression data reinforce the significance of the clastic nature of soil. The detailed examination of grain crushing and rearrangement in relation to stress-path simulations also begins to clarify the degree to which stress can sensibly be normalised by crushing strength, and the relationship that can be expected between crushing, yielding and plasticity in soils.

MODELLING OF AN AGGLOMERATE

Contact constitutive models

The PFC^{3D} program (Itasca Consulting Group, 1999) uses the soft contact approach of the distinct element method, which assumes that elements have a finite normal stiffness and represents elastic flattening at contacts by allowing the bodies to overlap. A stiffness model, a bonding model and a slip model are included in the constitutive representation of contact points between the elementary spheres that are the basic building blocks.

In the linear contact-stiffness model, the normal stiffness, K^n, and the shear tangent stiffness, K^s, at a contact are computed assuming that the stiffnesses of the two contacting objects act in series: that is, by

$$K^n = \frac{k_n^A k_n^B}{k_n^A + k_n^B},\ K^s = \frac{k_s^A k_s^B}{k_s^A + k_s^B} \tag{1}$$

where k_n^A and $k_n^B$are the normal stiffness of two objects A and B that are in contact, and k_s^A and k_s^B are the shear stiffnesses—both expressed as the force per unit displacement.

The simple contact bond can be envisaged as a pair of elastic springs at a point of glue. It serves to limit the total normal and shear forces that the contact can carry by enforcing bond-strength limits. The maximum tensile force that the bond can sustain in tension and the maximum shear force it can withstand before breaking are specified when the bond is created, and may be modified at any time during the simulation. The bond breaks if either of these values is exceeded. As the simple contact bond acts over a vanishingly small area of contact point, it does not resist bending moment. This means that it has no resistance to rolling of a sphere bonded adjacent to it if no third body exists to restrain the motion. This approach has been used by Robertson & Bolton (2001) and McDowell & Harireche (2002).

A slip model acts between unbonded objects in contact, or between bonded objects when their contact bond breaks. It limits the shear force between objects in contact, and allows slip to occur at a limiting shear force, governed by Coulomb's equation. The smaller of the friction coefficients of the two objects in contact is used to calculate the maximum shear force that the contact can sustain before sliding occurs:

$$F^s_{max} = \mu |F^n_i| \tag{2}$$

where F^s_{max} is the maximum allowable shear contact force, μ is the coefficient of friction, and F^n_i is the normal component of the contact force.

Agglomerates and crushing

Locked-in forces can arise if overlaps exist between spheres when bonding is applied; strain energy would then be released when the bond is broken. To avoid this effect the agglomerates were made from a regular assembly of spheres in hexagonal close packing (HCP), without initial overlap. As these agglomerates were intended to represent solid particles, the main purpose of the regular packing was to minimise the space between the spheres of the agglomerate (Robertson, 2000). However, in order to provide a statistical variability to the strength and shape of the agglomerates, similar to that of a real sand, each elementary sphere of an agglomerate was given a probability of existence of only 80% when it was created. As a result an average of 20% of the elementary spheres will not appear in the final agglomerate used for subsequent testing, about 11 spheres less than the maximum number of 57. Agglomerate details, which model the properties of a typical sand grain, are given in Table 1. Fig. 1 shows 20 typical 'grains'.

Randomly orientated agglomerates were then numerically crushed between two smooth and stiff platens under strain-controlled compression. The initial separation of the platens was the same as the size of the agglomerate, which was 1·0 mm. With the variability given to the agglomerates, different peak stresses were obtained from 20 tests. Fig. 2 shows a typical result from the crushing tests; it is compared with the crushing of a silica grain reported by Nakata *et al.* (2001). The diameter of the tested silica grain is 1·4–1·7 mm, which is slightly larger than that of the simulated agglomerate. The applied stress is calculated by normalising the platen force by the square of the initial diameter of the simulated agglomerate. A similarity in the response is found, in which both the computer simulation and the experimental single particle crushing test results produce lower peaks (at A, B and C in Fig. 2(a)) before the maximum peak stress (at D). After the agglomerate is split at the maximum stress, the platens continue to approach one another with low contact stresses until they find another good contact on the disintegrating agglomerate, to generate another split.

Table 1. Agglomerate details, modelling the properties of a typical sand grain

Input parameter	Numerical value
Diameter of agglomerate: mm	1·0
Diameter of sphere: mm	0·2
Density of sphere: kg/m^3	2650
Maximum number of spheres in agglomerate	57
Maximum number of bonds in agglomerate	228
Normal and shear bond strength: N	4
Normal and shear stiffness of each sphere: N/m	4×10^6
Frictional coefficient of sphere	0·5
Percentage of spheres removed at random: %	20

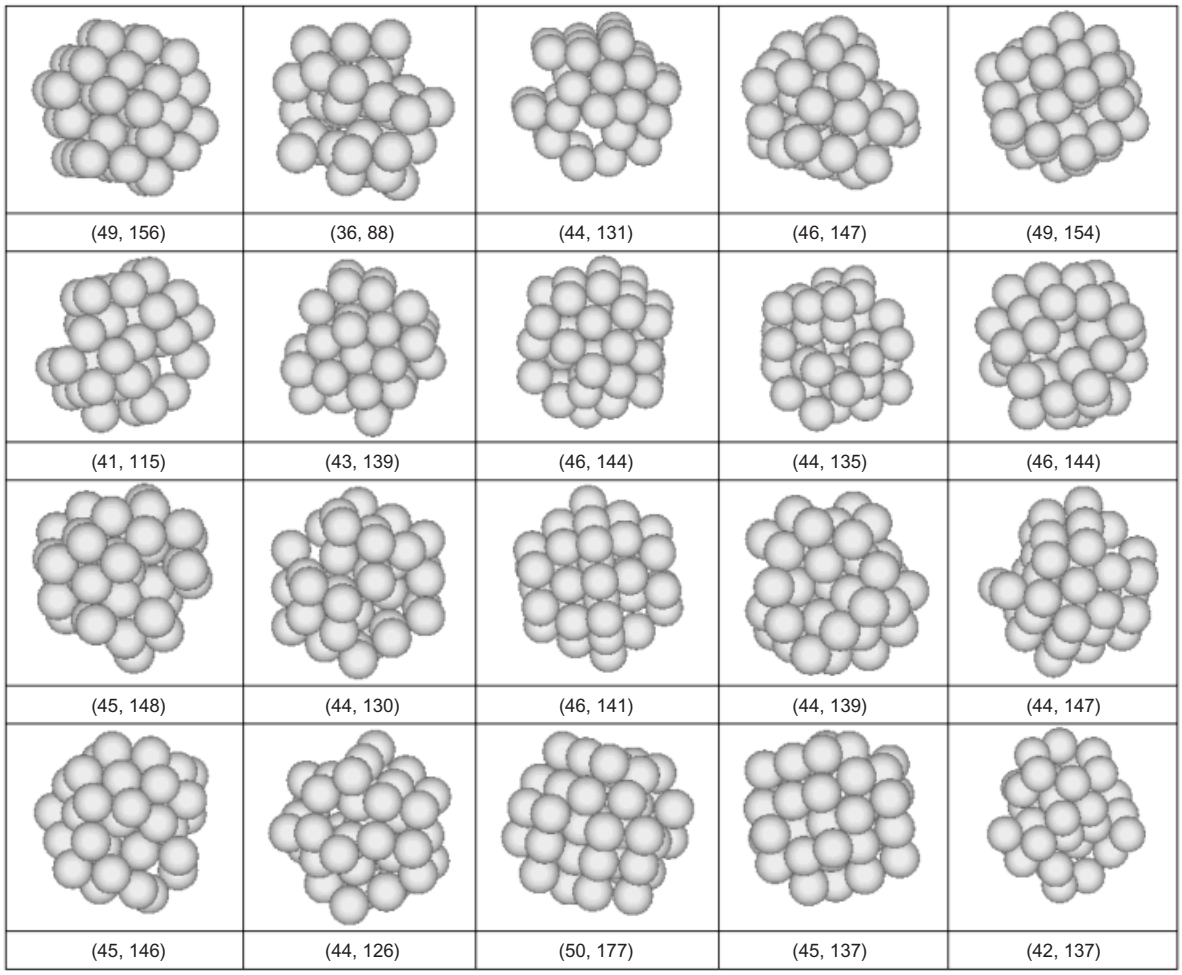

Fig. 1. Twenty typical 'grains' of single crushing tests

From the numerical simulation, we can also obtain information about the sequence of bond breakage in this specific agglomerate, which initially possessed 144 bonds connecting 46 spheres. Fig. 3 shows that no bonds break until the normal compressive stress reached 34 MPa. Comparing with Fig. 2(a), this demonstrates that the two initial peaks A and B simply represented rotation and slippage of the agglomerate in the platens. It must be recalled that the agglomerates are irregular (see Fig. 1), so that some readjustment of the position is inevitable. Figs 2(a) and 3 go on to show that the first drop in stress due to bond breakage is at point C, after seven of the bonds have broken. The subsequent drop in stress to 22 MPa between peaks C and D is accompanied by the breakage of seven additional bonds, bringing the total to 14. Breakage during unloading is an indicator of fracture propagation through the agglomerate. Apparently, this initial fracture did not create sufficient degrees of freedom to split the agglomerate. Instead, the stress first stabilised at 22 MPa and then increased again to 59 MPa as the platens continued to approach, during which time a further two bonds broke.

These two bonds must have been important interlocks, because the agglomerate then disintegrated, with a further 23 bonds breaking, bringing the total to 39. At that stage, there was a collection of fragments lying between the platens, and further crushing occurred, for example at E, as the platens continued to approach. In some cases the agglomerate remains in one cluster throughout the crushing despite crack propagation. This is attributed to the limited number of spheres restricting the formation of a clear fracture plane. It is suggested that bond breakage in Fig. 3 is a reasonable simulation of the internal fracture and external crushing in silica sand grains to which we attribute the similarity in behaviour between Fig. 2(a) and Fig. 2(b).

The procedure for the single agglomerate crushing is similar to that described by Robertson & Bolton (2001) except that an explicit dynamic analysis was used here, rather than PFC^{3D}'s quasi-static density-scaling routine. It was then possible, and necessary, to check that inertia-induced dynamic impact effects due to high loading rate had no significant effect on the crushing behaviour. Another agglomerate selected from Fig. 1 was numerically crushed under different approaching speeds of the platens. Fig. 4(a) shows that the peak stress of splitting the agglomerates is a function of the selected rate of compression, demonstrating that a computationally efficient platen speed of 1 m/s creates negligible extra strength. A higher strength is recorded at speeds in excess of 1 m/s due to inertial 'confinement', and a larger number of bonds are correspondingly broken (Fig. 4(b)). These inertia effects should also not be confused with rate effects due to creep at points of contact that hinder the study of equilibrium states in real sand. No attempt has been made to simulate contact creep in the present study.

Statistical interpretation

The survival probability of a batch of 20 agglomerates was calculated using the mean rank position (Davidge, 1979): that is,

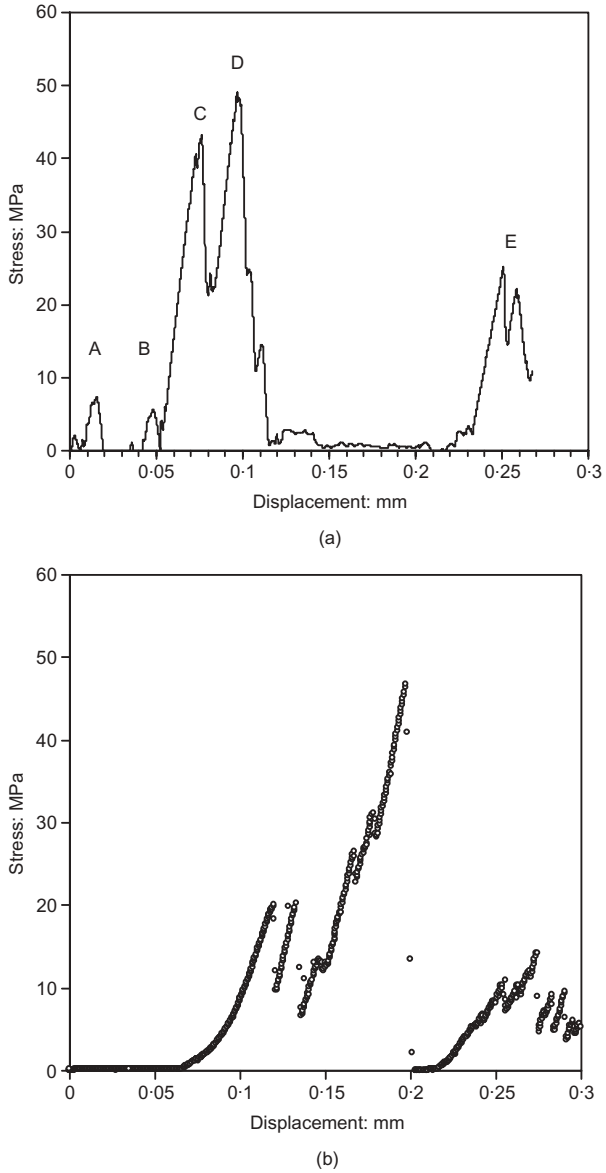

Fig. 2. Single-particle crushing test: (a) DEM simulation; (b) silica sand (Nakata *et al.*, 2001)

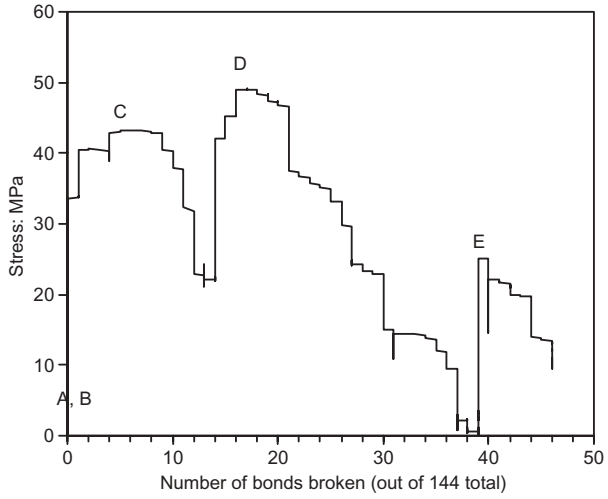

Fig. 3. Bond breakage of the agglomerate

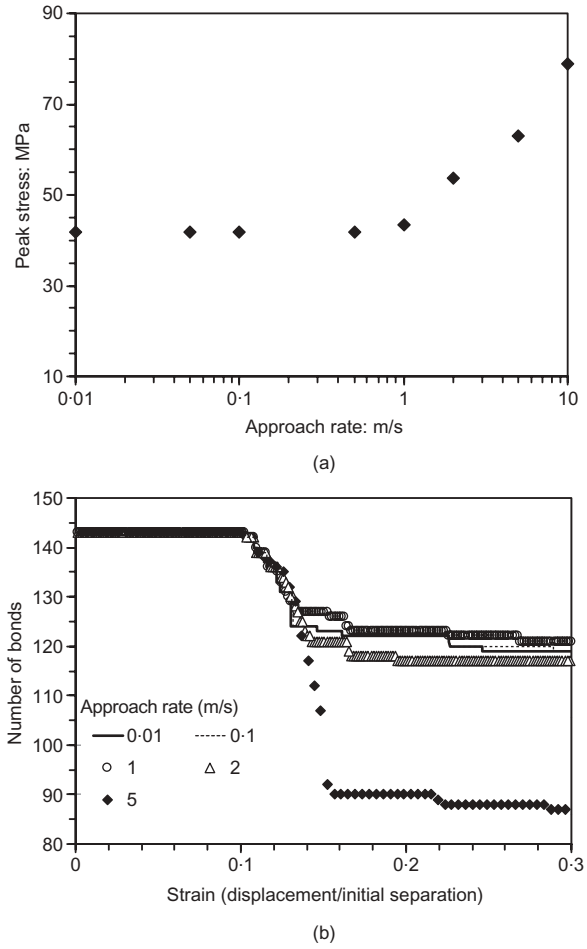

Fig. 4. Effect of platen speed on agglomerate crushing: (a) maximum force; (b) bond-breaking

$$P_s = 1 - \frac{i}{N+1} \tag{3}$$

in which i is the rank position of a grain when sorted into increasing order of peak stress, and where $N = 20$ here. The Weibull distribution can be used to describe the variability in tensile strengths of apparently identical test-pieces of a brittle material, in which the survival probability, P_s, is a function of normalised stress, σ/σ_0, given by

$$P_s = \exp\left[-\left(\frac{\sigma}{\sigma_0}\right)^m\right] \tag{4}$$

where σ_0 is the characteristic stress at which 1/e or 37% of samples survive and m is the Weibull modulus. McDowell & Bolton (1998) explain that a similar approach can be used on the compressive normalised strength, F/d^2, in grain-crushing tests treated as indirect tension tests, where F is the greatest force that is carried and d is the initial separation of the platens. Equation (4) can then be rewritten as:

$$\ln\left[\ln\left(\frac{1}{P_s}\right)\right] = m \ln\left(\frac{\sigma}{\sigma_0}\right) \tag{5}$$

and used to estimate a Weibull modulus for the sets of grains by carrying out a least-squares regression. The same procedure was used to estimate the Weibull modulus in the following tests, in which crushing tests were carried out on simulated particles containing random variations, as described.

Figure 5 shows that a similar shape of the survival probability curve is obtained when the crushing peak stress is normalised by σ_0, although the silica sand has $\sigma_0 =$ 31 MPa and the simulated agglomerate has $\sigma_0 = 80$ MPa. In addition, both of them give values of Weibull modulus of approximately 3. Robertson (2000) showed that the Weibull modulus of a flawed agglomerate depends on the proportion of spheres removed, or bonds weakened.

MODELLING A SOIL ELEMENT

Isotropic compression

For each of the numerical tests reported here, an initial set of 'exo-spheres' was first created at a size slightly smaller than the required agglomerates given in Table 1. They were placed at random, but excluding overlaps. Then they were expanded to the required size of 1 mm, and cycled to equilibrium so as to reduce unwanted gaps. During this process shear stiffness and friction were reduced to zero, while normal stiffness was increased 100-fold. Following Robertson (2000), a linked list storing the coordinates of their centres was then created and the exo-spheres were deleted. Randomly rotated aggregates were then created in their place, centred at the coordinates in the list, and the assembly was cycled to equilibrium again before commencing the tests. To reduce the likelihood of bonds between balls breaking during this stage, the strengths of the bonds were initially set very high and reduced after a number of cycles. The final shear and normal stiffnesses of the balls of the agglomerates were set to their final values ($4{\cdot}0 \times 10^6$ N/m) and their coefficient of friction was set to 0·5 (corresponding to a contact friction angle of 26·5°). Finally, bond strengths were fixed and variability was provided in order to achieve the required statistical distribution of breakage strength. Approximately 2% of the total number of bonds broke during the final stages of this sample preparation process. The equilibrium stress at this stage was 20 kPa, although the maximum stress recorded was as high as 1 MPa.

The cubical arrangement of 389 agglomerates shown in Fig. 6 was then isotropically compressed to 0·1 MPa by moving one pair of walls progressively together and continuously adjusting the position of the other two pairs of walls to achieve an isotropic stress path. A wall speed of 0·01 m/s was slow enough to eliminate rate effects due to bouncing of any initially unloaded agglomerates. Here, 'stress' is calculated from the summation and averaging of all contact forces on a parallel pair of walls. The voids ratio, calculated by using the solid volume as the total volume of the spheres, was at this stage 2·1, shown as the initial condition in Fig. 7(a).

Strain-controlled loading then continued at higher speeds from 0·5 m/s to 2 m/s to check for possible inertia effects on the location of the virgin compression line. There is a noticeable dynamic effect on the compression behaviour above 1 m/s in Fig. 7. When the soil element was numerically compressed at a higher rate, the strength of individual agglomerates would become higher, as seen in Fig. 4, and grains would therefore start crushing at a higher stress level. As can be seen, the 2 m/s rate shifted the virgin compression line to the right even when the curve reached the linear fractal compression zone, leading to a different amount of bond breakage (Fig. 7(b)).

The initial phase of irrecoverable compression beyond 1 MPa in Fig. 7(a) happens before any significant breakage, as can be seen in Fig. 7(b), and must therefore be attributed to re-packing due to elastic compression at points of contact permitting sliding, similar to the peaks (A and B) observed in Fig. 2. Breakage starts at approximately 8 MPa, approximately a tenth of the characteristic breakage strength of agglomerates tested between platens. The higher coordination number in this case, because of the nearby supporting agglomerates, should reduce the induced tensile stresses (McDowell & Bolton, 1998). So an agglomerate within a soil element might have been expected to break at an applied stress even higher than the strength exhibited

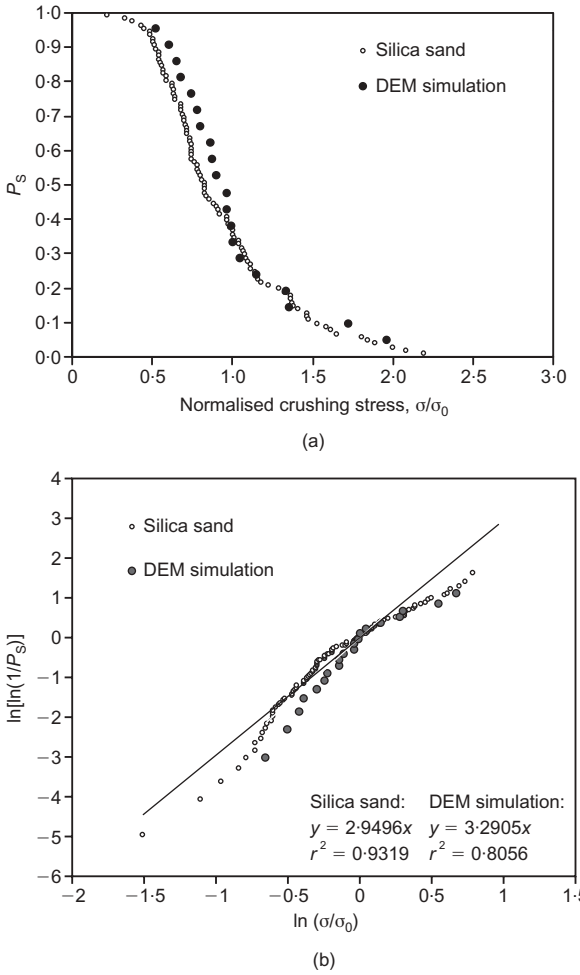

Fig. 5. Survival distribution curve of single agglomerate crushing: (a) normalised distribution; (b) Weibull modulus

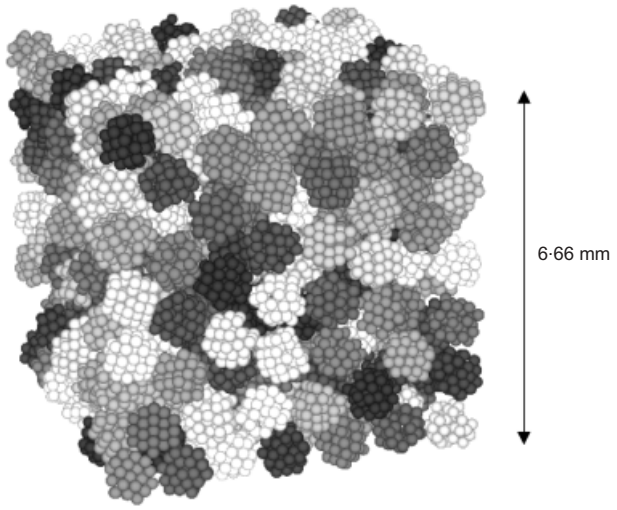

Fig. 6. Cubical arrangement of 389 agglomerates

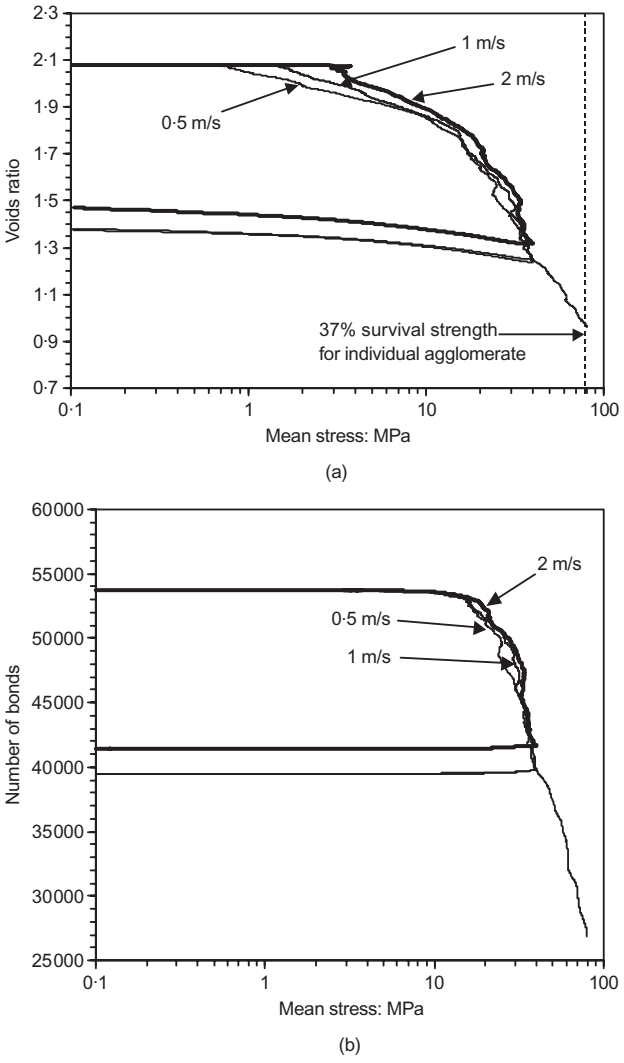

Fig. 7. Effect of compression rate on isotropic compression and swelling curve: (a) voids ratio against $\log p'$; (b) bond breakage against $\log p'$

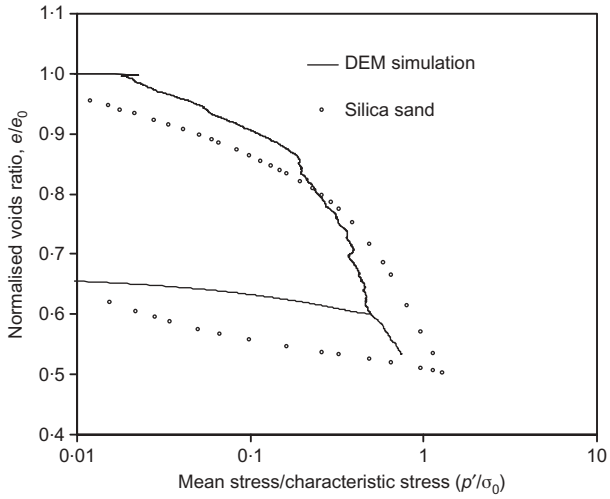

Fig. 8. Normalised isotropic compression curves

between two platens. This tendency must have been counteracted by order-of-magnitude stress concentrations acting on individual agglomerates. Concentrated force chains have been observed experimentally (Oda & Konishi, 1974) and in DEM simulations (Cundall & Strack, 1979). When the linear logarithmic compression line is reached at approximately 15 MPa, Fig. 7 shows a similar linear bond breakage plot against the logarithm of mean stress, which provides an interesting coincidence between the micro and macro behaviour of the simulated soil as it clastically compresses.

The swelling curve of the computer soil element is inelastic. Bond breakage occurs at the beginning of swelling, then no further bonds break. This computed further bond breakage must be due to rearrangements that over-stress exposed 'asperities' even though the macroscopic stress is falling. This creates some hysteresis as well as continued volume reduction when more load–unload loops are applied. The unloading loop would presumably better resemble that of the real sand if the sand grains possessed the same extraordinary surface profile as the agglomerates. The overall shape of the loop, whether concave up or concave down, is mainly a matter of selecting a contact-stiffness model—here simply linear. However, the overconsolidation cycle is not the main interest of this paper.

Figure 8 shows a comparison of isotropic compression curves between the silica sand and the DEM simulation with a platen speed of 1 m/s. The silica sand has a more gentle transition into what may be described as clastic compression. One explanation is that the real sand particles have a greater variety of sizes and asperities, compared with the agglomerates in the DEM simulation. The opportunities for both elastic compression and crushing on strong force chains will be more variable. Similarly, the 'normal compression line' in the DEM simulation begins to stiffen below a normalised voids ratio of 0·6, in contrast to the real sand. This is also tentatively attributed to the fact that agglomerates have only a limited number of component spheres. When approximately 30% of bonds have been broken (after 40 MPa), as indicated by Fig. 7, it might be argued that the real sand has more opportunity to continue fragmenting. Ideally, agglomerates would be modelled with an order of magnitude more spheres so that they were the same size as the comminution limit of silica sands, perhaps 1 μm (Kendall, 1978), but this would increase the computation time unrealistically.

Stress path tests and critical states

Various stress path triaxial compression tests were then simulated in the cubical cell, from different stress levels on the isotropic virgin compression line. One advantage of computer simulation is that the storage of data files makes it possible to reproduce sample initialisations exactly; another is that tests can be conducted to very large strain levels. The positions of the walls confining the minor and intermediate principal axes were adjusted continually in relation to the force they were required to carry, using appropriate feedback algorithms. In other words, the simulation was similar to a laboratory triaxial test in its force and displacement control. Constant-volume tests (e = constant), conventional triaxial 'drained' compression tests with constant lateral principal effective stress ($\sigma'_3 =$ constant) and constant mean effective pressure tests (p' = constant) were all simulated.

Triaxial compression tests on real silica sand and DEM simulations on agglomerates are compared in Fig. 9 for the cases $\sigma'_3 = 10$ MPa and $\sigma'_3 = 20$ MPa. It is seen that the DEM simulations are broadly consistent with reality. In every test, the deviator stress approaches a plateau while volume continues to decrease as bonds continue to break. Although this conjunction conflicts with the simple precepts of stress-dilatancy theories, it does conform with the real data of crushable sands. In more detail, both the mobilised deviator stress and the corresponding volumetric strain in the real sand are overestimated in the DEM simulations by

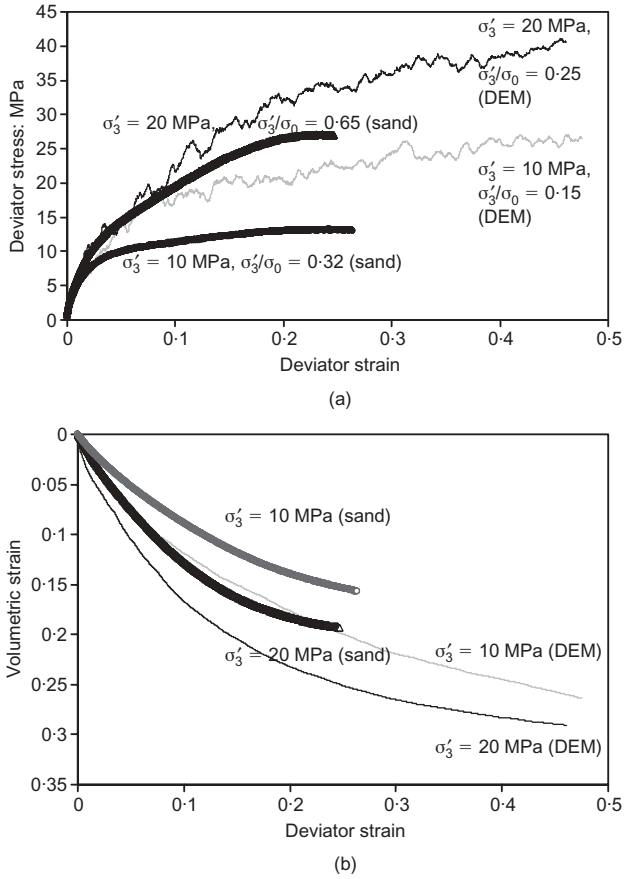

Fig. 9. Conventional triaxial test: (a) stress against strain; (b) volumetric strain against deviator strain

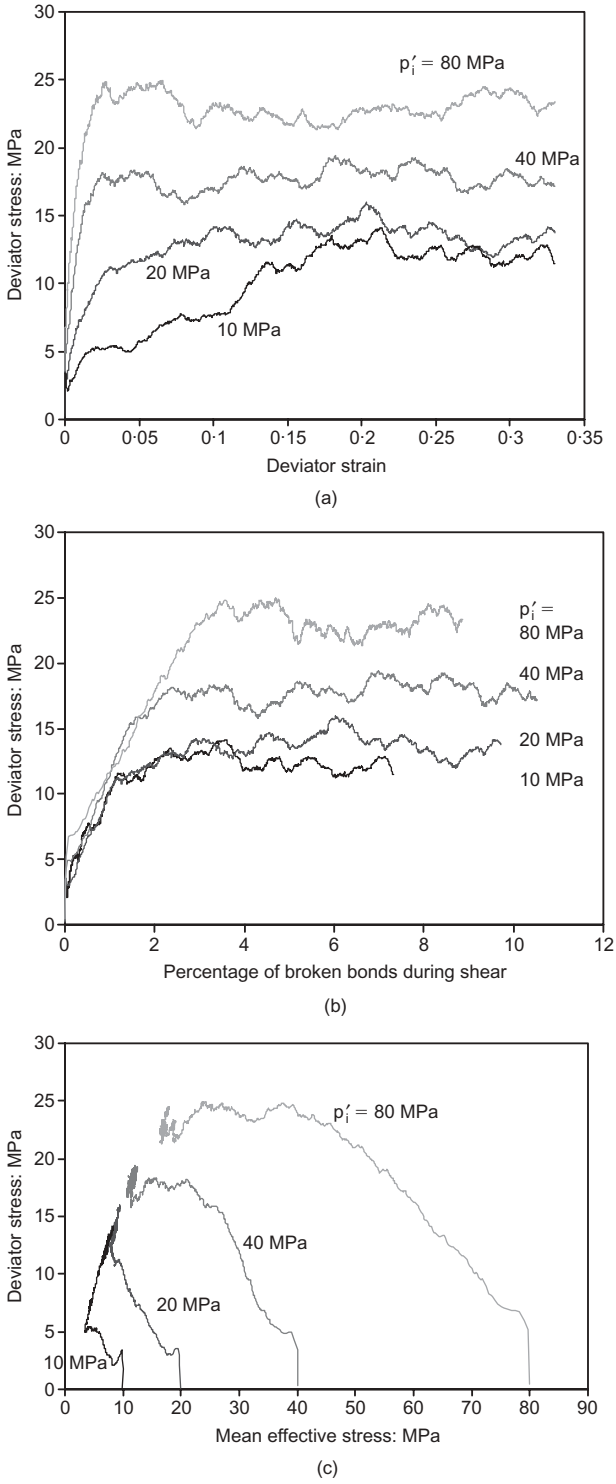

Fig. 10. DEM simulation of constant-volume tests: (a) stress against strain; (b) stress against percentage broken bonds; (c) stress paths

factors of about 1·2–1·4, whereas the characteristic stress of the DEM agglomerates is higher than that of the silica sand by a factor of 2·6.

Figure 10 shows constant-volume ('undrained') test results as stress–strain plots in (a), stress-breakage in (b) and effective stress-path plots in (c). The percentage of bond breakage is defined as the number of bonds broken during shearing divided by the initial number of bonds existing at the initial effective mean stress level, p'_i, of the respective test. In every case the deviator stress first increases to about 3–5 MPa with no additional bond breakage, and the stress path rises at constant p', as would be expected for an elastic granular material. Bonds then begin to break. Fig. 3 shows that breakage of bonds was only occurring in a single agglomerate after 34 MPa of macroscopic stress. This again suggests that order-of-magnitude stress fluctuations crush some agglomerates.

The second stage in each test consists of small but significant amounts of continuing breakage as the mean effective stress roughly halves, while the deviator stress increases. If these simulations were a real undrained test on sand, the excess pore water pressure would be rising during this stage, at a rate $\delta u/\delta q$ in the range 1–2. This would probably be seen as the effect of suppressed compaction during shear. This compaction effect arises from grain crushing, which permits the aggregate to pack more efficiently, and therefore permits all elastic contacts to relax in order to maintain overall constant volume. This second phase of grain damage seems to finish in all these simulations at a deviator strain, ε_q, of about 2·5%, as shown by comparing Fig. 10(a) and Fig. 10(c). The subsequent behaviour is very dependent on the initial effective stress level, p'_i.

The results from low initial stresses ($p'_i < 40$ MPa corresponding to $p'_i/\sigma_0 < 0{\cdot}5$ in terms of the characteristic grain strength, $\sigma_0 = 80$ MPa) show the classic undrained behaviour of a medium-dense sand in stage 3, starting with the 2·5% strain level representing a point of 'phase transformation' (Ishihara *et al.*, 1975), or 'quasi steady state' (Alarcon-Guzman *et al.*, 1988), at which the rate of change of mean effective stress reverses, and after which there is further strength gain due to suppressed dilatancy. This dilatancy arises from the rearrangement of the interlocked

agglomerates due to shearing, and it more than compensates for any ongoing crushing, so that additional compression of elastic contacts is required to achieve overall constancy of volume, and p' rises accordingly. A high stress ratio (q/p') is required to achieve this ongoing rearrangement, but as p' rises the amount of breakage increases and the strength levels off as compaction due to crushing offsets dilatant rearrangement. This might be regarded as a curved line of failure states with $q/p' \approx 1{\cdot}81$, $1{\cdot}74$ and $1{\cdot}67$ in the 10, 20 and 40 MPa tests respectively. The corresponding fall in ϕ_{max} from 44° to 41° is similar to that described by Bolton (1986) as being due to particle crushing.

In contrast, the simulations starting from high stresses ($p'_i > 40$ MPa, $p'_i/\sigma_0 > 0{\cdot}5$) are initially stiffer, presumably because the aggregate is denser and more strongly interlocked. They reach a peak strength at about 2·5% deviator strain after stage 2, but the deviator stress then drops slightly in stage 3 to a minimum of about 17 MPa for $p'_i = 40$ MPa (or $q/\sigma_0 \approx 0{\cdot}21$) and about 22 MPa for $p'_i = 80$ MPa (or $q/\sigma_0 \approx 0{\cdot}28$) at 10% deviator strain, corresponding to a quasi-critical stress ratio, $M \approx 1{\cdot}40$ (or $\phi_{crit} \approx 34{\cdot}5°$). Strength then fluctuates slightly at roughly the same stress ratio.

There is some ambiguity in the location of a critical-state line on the plot of e against $\log p'$ in Fig. 11. The whole series of drained and undrained test paths is shown, together with indicative arrows when the final state of the simulation was continuing to change when the computation was terminated. In particular, the drained test with $\sigma'_3 = 20$ MPa was continuing to reduce in volume as bonds continued to break, even at 50% deviator strain. Nevertheless, there is some suggestion that a critical-state line exists about one unit of natural logarithms inside the fully developed normal compression line, just as critical-state soil mechanics suggests. The simulations also suggest that the dissipation function used in Cam clay might be improved if grain damage and grain rearrangement were recognised as distinct micro-mechanisms, perhaps following the logic of Chandler (1985).

The significance of what has been achieved with these DEM simulations would be diminished if the output of Figs 9, 10 and 11 did not so closely resemble the data for real granular materials. Fig. 12 shows the undrained test data of Yamamuro & Lade (1993) and Lade & Yamamuro (1996) for Cambria sand, for comparison with the simulations in Fig. 10(c). Both figures show that the peak deviator stress appears at approximately half the initial confining pressure.

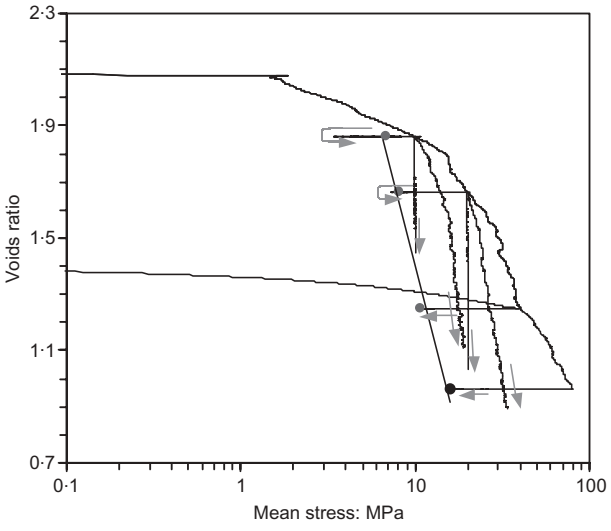

Fig. 11. Critical state line estimated from DEM simulation

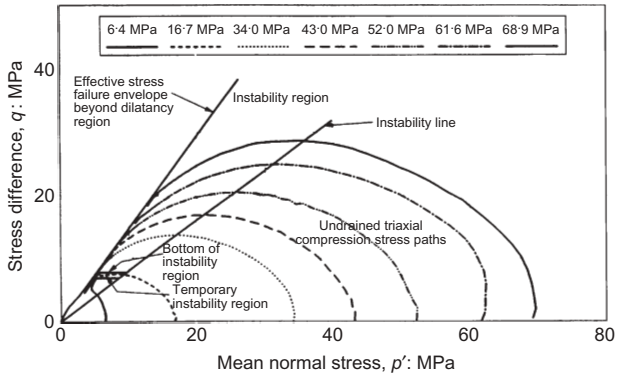

Fig. 12. Undrained triaxial compression test results (Yamamuro & Lade, 1993)

Then the deviator stress falls to reach the phase transformation point, after which it increases again at constant stress ratio before the critical state is reached.

CONCLUSIONS

(*a*) Distinct element models have, for the first time, been shown to be capable of replicating the complex behaviour of sands in relation to their strength, dilatancy, and critical states. This has been achieved by introducing the idea that a grain can be considered to be an agglomerate of bonded micro-elements, here represented as spheres.

(*b*) The omission of a small percentage of micro-elements has been shown to be capable of creating a lifelike distribution of grain crushing strengths, with a typical Weibull modulus of 3 being associated with 20% of such 'flaws'. The spread of strengths between grains, and comparison of asperities and of the whole grains, is very significant in creating a reasonable representation of stress-level effects in soils.

(*c*) Once a lifelike spread of crushing strengths has been achieved, the behaviour of aggregates of grains can be represented as a function of the normalised mean effective stress level, p'_i/σ_0. As soil progresses down its virgin compression line, grain crushing leads to hardening in the sense that fragments become less free to fracture again. This is the nature of the 'normal compression line', although the fractal hardening of real granular materials cannot be replicated in agglomerates containing only a limited number of identical micro-spheres.

(*d*) Test simulations were conducted at wall velocities up to about 1 m/s without inertia effects creating false 'strength' through unwanted 'confinement'.

(*e*) Realistic 'drained' and 'undrained' test path behaviour of sands can be simulated. Samples taken first to $p'_i/\sigma_0 \approx 1$ show some brittleness in undrained tests, but nevertheless then converge on high-strength critical states. Notwithstanding the tendency for pore pressure generation, crushing virgin soils are stable in monotonic shearing. Samples pre-consolidated only to $p'_i/\sigma_0 \approx 0{\cdot}1$ show initial loss of effective stress on 'undrained' shearing as damage takes place, but they then pass through a 'phase transition' and lock up again, gaining undrained strength as the agglomerate grains attempt to dilate.

(*f*) Confusions and ambiguities arising from the concepts of phase transformation, quasi steady state, critical state, cyclic mobility and soil liquefaction should be able to be

resolved by further DEM simulations in which constitutive parameters can be varied, cyclic stresses applied, and heterogeneous soil structures created by removing a proportion of agglomerates prior to shearing.

(*g*) Attention to the actual micromechanics of granular interactions should lead to improved continuum soil models.

ACKNOWLEDGEMENTS

Yukio Nakata is pleased to acknowledge the support of the Japanese Society for the Promotion of Science, and of Yamaguchi University, in facilitating his period of leave at Cambridge University. Yi-Pik Cheng is grateful for support from the Croucher Foundation of Hong Kong.

NOTATION

d	initial separation of two platens
e	voids ratio
e	exponential function
F	greatest force carried by a grain between two platens
$F^{\mathrm{s}}_{\mathrm{max}}$	maximum allowable shear contact force
$F^{\mathrm{n}}_{\mathrm{i}}$	normal component of contact force
i	rank position of a grain when sorted into increasing order of peak stress
$K_{0,\mathrm{nc}}$	earth pressure coefficient at rest for normally compressed soil
$k^{\mathrm{A,B}}_{\mathrm{n}}$	normal contact stiffness of a sphere, A or B
$k^{\mathrm{A,B}}_{\mathrm{s}}$	shear contact stiffness of a sphere, A or B
K^{n}	normal contact stiffness at contact point between two spheres
K^{s}	shear contact stiffness at contact point between two spheres
m	Weibull modulus
M	slope of critical-state line
N	number of agglomerates or sand grains
p'	mean effective stress
p'_{i}	initial mean effective stress before shearing test
P_{s}	survival probability of a grain
q	deviator stress, $\sigma'_1 - \sigma'_3$
δu	change in excess pore water pressure
δq	change in deviatoric stress
ε_{q}	deviator strain, $2/3(\varepsilon_1 - \varepsilon_3)$
ϕ	angle of shearing resistance
ϕ_{crit}	critical-state angle of shearing resistance
ϕ_{max}	peak mobilised angle of shearing resistance
μ	coefficient of friction of sphere
σ	stress acting on a grain
σ'_1	major stress acting on cubical sample or triaxial cell
σ'_3	minor pressure acting on cubical sample or triaxial cell
σ_0	characteristic stress (strength) at which $1/e$ or 37% of a batch of agglomerates survive

REFERENCES

Alarcon-Guzman, A., Leonards, G. A. & Chameau, J. L. (1988). Undrained monotonic and cyclic strength of sands. *J. Geotech. Engng Div., ASCE* **114**, No. GT10, 1089–1109.

Been, K. & Jefferies, M. G. (1985). A state parameter for sands. *Géotechnique* **35**, No. 2, 99–112.

Bolton, M. D. (1986). The strength and dilatancy of sands. *Géotechnique* **36**, No. 1, 65–78.

Castro, G. & Poulos, S. J. (1977). Factors affecting liquefaction and cyclic mobility. *J. Geotech. Engng Div., ASCE* **103**, No. 6, 501–516.

Chandler, H. W. (1985). A plasticity theory without Drucker's postulate, suitable for granular materials. *J. Mech. Phys. Solids* **33**, No. 3, 215–226.

Cheng, Y. P., White, D. J., Bowman, E. T., Bolton, M. D. & Soga, K. (2001). The observation of soil microstructure under load. *Proc. Powders and Grains 2001*, *Sendai*, 69–72.

Cuccovillo, T. & Coop, M. R. (1999). On the mechanics of structured sands *Géotechnique* **49**, No. 6, 741–760.

Cundall, P. A., & Strack, O. D. L. (1979). A discrete numerical model for granular assemblies. *Géotechnique* **29**, No. 1, 47–65.

Davidge, R. W. (1979) *Mechanical behaviour of ceramics*. Cambridge: Cambridge University Press.

Hoque, E., Tatsuoka, F. & Sato, T. (1996). Measuring anisotropic elastic properties of sand using a large triaxial specimen. *Geotech. Test. J.* **19**, No. 4, 411–420.

Ishihara, K., Tatsuoka, F. & Yasuda, S. (1975). Undrained deformation and liquefaction of sand under cyclic stresses. *Soils Found.* **15**, No. 1, 29–44.

Itasca Consulting Group, Inc. (1999) *PFC^{3D} (Particle Flow Code in Three Dimensions)*, Version 2·00. Minneapolis: ICG.

Kendall, K. (1978). The impossibility of comminuting small particles by compression. *Nature* **272**, 710–711.

Lade, P. V. & Yamamuro, J. A. (1996). Undrained sand behaviour in axisymmetric tests at high pressures. *J. Geotech. Eng., ASCE* **122**, No. 2, 120–129.

McDowell, G. R. & Bolton, M. D. (1998). On the micromechanics of crushable aggregates. *Géotechnique* **48**, No. 5, 667–679.

McDowell, G. R., Bolton, M. D. & Robertson, D. (1996). The fractal crushing of granular materials. *Int. J. Mech. Phys. Solids* **44**, 2079–2102.

McDowell, G. R. & Harireche, O. (2002) Discrete element modelling of soil particle fracture. *Géotechnique* **52**, No. 2, 131–135.

Nakata, Y., Kato,Y., Hyodo M., Hyde, A. L. & Murata, H. (2001). One-dimensional compression behaviour of uniformly graded sand related to single particle crushing strength. *Soils Found.* **41**, No. 2, 39–51.

Oda, M. & Konishi, J. (1974). Microscopic deformation mechanism of granular material in simple shear. *Soils Found.* **14**, No. 4, 25–38.

Robertson, D. (2000). *Computer simulations of crushable aggregates*. PhD dissertation, Cambridge University.

Robertson, D. & Bolton, M. D. (2001). DEM simulations of crushable grains and soils. *Proc. Powders and Grains 2001, Sendai*, 623–626.

Thornton, C. (2000). Numerical simulations of deviatoric shear deformation of granular media. *Géotechnique* **50**, No. 1, 43–53.

Yamamuro, J. A. & Lade, P. V. (1993). Effects of strain rate on instability of granular soils. *Geotech. Test. J.* **16**, No. 3, 304–313.

Yasufuku, N. & Hyde, A. F. L. (1995). Pile end-bearing capacity in crushable sands *Géotechnique* **45**, No. 4, 663–676.